

2D Electrical Resistivity Tomography (ERT) Survey using the Multi-Electrode Gradient Array at the Bosumtwi Impact Crater, Ghana

Akwasi Acheampong Aning^{1,2*}, Piotr Tucholka¹, Sylvester K. Danuor²

1. Departement des Sciences de la Terre, Université Paris-Sud, Bat 504, F-91405 Orsay Cedex, France
2. Department of Physics, Kwame Nkrumah University of Science and Technology, Kumasi, Ghana

* E-mail of the corresponding author: acheamponganing@gmail.com

Abstract

The 10.5 km diameter Bosumtwi impact crater in Ghana is occupied by a lake of about 8.5 km in diameter. The multi-electrode gradient array has been used to carry out 2D electrical resistivity tomography (ERT) survey at different locations around the crater. The 2 m take-out cable of the ABEM LUND Resistivity Imaging System was modified to function as a 5 m take-out. 2D electrical resistivity survey was carried out along six (6) radial profiles running from the shore of the lake towards the crater rim. The least-square inversion technique was used to invert the topographically corrected data. The area extending from the lake shore towards the crater rim contains essentially three formations: the low resistivity regions from the shore of the lake towards uphill with resistivities $< 64 \Omega.m$ representing the lake sediments; the moderately high resistivity regions with values between 128 and 200 $\Omega.m$ interpreted as impact related breccias such as dikes, allochthonous or parautochthonous depending on their geometries; lastly, the model clearly differentiates the resistive basement metamorphic rocks of resistivities $> 128 \Omega.m$ from the lake sediments and the breccias due to their geometry and lateral extent. The ERT models allowed us to locate faults and fractures and also the thickness of the post impact lake sediments and the breccias. The results showed that the cables take-outs of the multi-core cable can be modified to suit the requirements of a particular survey thus highlighting the utility of this technique in impact cratering studies and geo-electrical imaging studies in general.

Keywords: impact crater, target rock, electrical resistivity tomography (ERT), multi-electrode gradient array, roll-along technique

1. Introduction

Most applications in geophysics require high resolution subsurface resistivity information in 2D and 3D. In the Electrical Resistivity Tomography (ERT) method, the sounding and the profiling techniques are integrated to give information on both the lateral and vertical extent of the subsurface. The ERT gives images either in 2D or 3D depending on how the data is acquired. Electrical resistivity imaging is popular nowadays due to its ability to produce images of the subsurface efficiently and effectively as a result of the availability of automated data acquisition systems and efficient user friendly inversion softwares. Figure 1 shows the arrangement of the electrodes, cables and the resistivity meter and the image obtained of a typical high resolution 2D resistivity survey.

ERT surveys can be carried out using different electrode arrays, such as gradient, square, dipole-dipole, Wenner, Schlumberger, etc. The electrodes are placed on the surface to send the electric current into the ground and the resulting voltage signals generated as a result are measured. It has been used to investigate areas of complex geology, such as volcanic and geothermal areas, landslides, seismotectonic structures, and areas of hydro-geologic phenomena and environmental problems and the deposition and flow of impact melt and breccias (Steeple, 2001; Colangelo et al., 2008; Lapenna et al., 2005; Griffiths and Barker, 1993; Tong et al., 2010).

With the development of innovative and robust inversion methods incorporating topography, accurate data interpretation for resolving complex geological problems, such as defining aspects of hidden underground structures (i.e. fractures, water accumulations, etc.) or studying the spatiotemporal evolution of groundwater flow relative to landslide phenomena has become easier (Gunther et al., 2006; Loke and Barker, 1996). In the multi-electrode gradient survey, a number of electrodes are arranged in a straight line and attached to a multi-core cable (Figure 1). The potential electrodes are always within the current electrodes (Figure 2).

The current is injected into the subsurface using a separation of $(s + 2)a$ and all the corresponding voltages with potential electrodes spacing of a are measured simultaneously. s is an integer, and it gives the maximum number of potential readings for a current injection, and it also gives the maximum separation between the potential

electrodes. The midpoint of the potential dipole m relative to the current pair electrodes is given as:

$$m = \frac{\frac{(x_M + x_N)}{2} - \frac{(x_A + x_B)}{2}}{(x_N - x_M)} = \frac{(x_{MN} + x_{AB})}{a} \dots \dots \dots 1$$

where x_A, x_B, x_M, x_N are the positions of the current and potential electrodes, and $x_B > x_A, x_N > x_M$ and x_{AB}, x_{MN} are the midpoints of the respective dipoles. m can also be evaluated from the relation $m = n - (s + 1) = 2$, for $x_{MN} \leq x_{AB}$ ($m \leq 0$) for and $m = n + (s + 1) = 2$, for $x_{MN} \geq x_{AB}$ ($m > 0$), where n and m are negative or positive integers (Dahlin and Zhou, 2006).

This paper reports on how the ABEM 2 m cable take-out was innovatively modified to function as a 5 m take-out, and then used to map the subsurface structure of the Bosumtwi impact crater.

2. Geological Background of the Study Area

The Bosumtwi impact crater (Figure 3) located in Ghana is centered at $06^{\circ} 32' N, 01^{\circ} 25' W$. It is one of the youngest well-preserved complex impact craters known on Earth and one of the 19 confirmed impact structures in Africa. The crater was dugout in lower green-schist facies meta-sediments of the 2.1 - 2.2 Ga Birimian Super-group about 1.07 Myr ago (Koeberl and Reimold, 2005). The meta-sediments consist of inter bedded phyllites/mica-schists and meta-tuffs, metagreywackes, quartzitic greywackes, shales and slates and these are intruded by small dikes and pods of granitic intrusives (Koeberl and Reimold, 2005). The 10.5 km diameter crater is almost completely filled by the 8.5 km lake which has a depth of about 75 m (Scholz, 2007, Karp et al., 2002). Moon and Mason (1967) mapped granitoid intrusions. Carbonate (calcite) which was previously unknown was identified in high abundance in the analysis of drill cores, and their origin is pre-impact (Coney et al., 2007; Deutsch et al., 2007; Ferrière et al., 2007). There are three types of impact breccia at the Bosumtwi crater area: an autochthonous monomict breccia, a probable allochthonous polymict lithic impact breccia, and a suevitic breccia based on their composition and texture (Boamah and Koeberl, 2003).

The complex crater has a central uplift with a width of 1.9 km in NW – SE direction and a maximum height of 130 m above the crater moat and it is surrounded by about 300 m thick post impact lacustrine sediments. The faulted central uplift has an irregular upper surface with a small graben structure that is 15 m deep and the faults extend about 120 m into the sediments. The uplift is located away from the center by about 1 km to the north of the center of the crater (Karp et al., 2002; Scholz et al., 2007).

3. Modification of the ABEM 2 m cable take-out

The ABEM LUND Resistivity Imaging System was the equipment that was used for this research. The electrode cable system available was four 21 take-out cables spaced every 2 m (Figure 4a). When all the four cables were connected, the total length was 160 m and this could only probe to a depth of about 30 m. It was necessary to find a way to increase the length of these cables since it was practically difficult to acquire new extended set. A design (Figure 4b) was created and wires were made. In the fabrication, about 3.3 km of wire were cut into different lengths. These wires were joined to the take-outs of the original ABEM electrode cables to get electrode separation of 5 m and a total length of 400 m in order to probe to a depth of about 75 m.

Wires were not cut for take-out *twenty one* of cable 1 and take-out *one* of cable 2 because these were the measurement stations and they were to be connected to the station electrode. The lengths of wires cut were a meter longer than the actual separation between the cable take-out and the electrode; this was to compensate for the varied topography. As an example (Figure 5a), take-outs *eleven* of the inner cables (2 and 3) would be 20 m away from the station but their corresponding electrodes would be 50 m away. Wires of length 31 m were cut to make up the difference in separation of 30 m. The lengths of wires for the take-outs *twenty one* of cable 1 and *one* of cable 2 and take-outs *twenty one* of cable 3 and *one* of cable 4 were the same (61 m) because they were to be connected to the electrodes 11 and 31 which are equally spaced from the center (Figures 5a and 5b).

The lengths of the wires that were added to the four cable take-outs are as shown in Tables 1 and 2 and they were based on the selected protocols. The multi-electrode gradient array was used for acquiring the data and the GRAD4LX8 and GRAD4S8 protocols were selected. For the GRAD4LX8 protocol (long layout), all the four cables would be used and only the odd-numbered take-outs would be connected for the measurements (Figures 5b and 6). The take-out separation for the odd-numbered take-outs of the 2 m take-out ABEM cables are 4 m but the electrodes were to be 10 m apart so there was the need to add wires to make up for the differences. For the GRAD4S8 protocol (short layout), only the inner cables were to be employed for the measurements and all the take-outs were to be used (Figures 5a and 6). The cable take-out separation is 2 m and the electrode spacing for this arrangement was to be 5 m. Two each of the same length of wire were cut for each of the protocols

GRAD4LX8 and GRAD4S8, one for cables on the left side of the station of measurements and the other for those on the right side.

The wires to be connected to each cable were carefully put together. In all there were four bundles, two each for the inner and outer cables. There were 20 wires in the bundles for the inner cables and 11 wires in that for the outer cables (Tables 1 and 2). The take-outs of the bundles of wires for the two ends were different because one end is to be connected to the ABEM cable and the other end to the electrodes. For the bundles of wires for the inner cable, the take-out of the end that is to be connected to the cable is 2 m whereas that for the electrodes is 5 m, and for the outer cables it is 4 m and 10 m respectively for the cable and the electrodes.

4. Data Acquisition and Processing

Resistivity imaging was carried out along six (6) lines radially around the lake. The profiles start from the shore and go uphill towards the rim of the crater. The resistivity measurements were performed with the modified multi-electrode ABEM Lund Imaging System which operates automatically once the geometrical parameters (array type, protocols, minimum electrode spacing, current) are set. The data acquisition was done in the multi-channel mode where for each current injection, the system takes multiple potential readings. The GRAD4LX8 and GRAD4S8 gradient array protocols were used for this four channel measurements in that order. The GRAD4LX8 was for the long layout (Figures 5b and 6) and all the four electrode cables were connected. The GRAD4LX8 was chosen because apart from the fact that it gives a dense near-surface cover and a slightly sparser measurement pattern at long electrode spacings, this protocol also takes Wenner-Schlumberger measurements data for the longest electrode separations in order to improve the resolution for the largest investigation depths which is necessary for this work (ABEM, 2008). The GRAD4S8 is for the short lay out (cables 2 and 3) (Figures 5a and 6) and is designed to supplement GRAD4LX8 data to enhance near surface resolution. All the electrode take-outs were connected in the GRAD4S8 protocol. The resistivity meter automatically switches the electrodes to serve as current or potential pairs. The selection of the protocols and the other inputs were done prior to going to the field.

The protocol file with *ORG* filename (Table 3) was used for the first set of measurements on every profile and the file with *UP* filename was used for the roll-along towards the rim. The data for the *UP* files was lower because of data overlap with the previous measurements (using the *ORG* file) and as a result measuring was much faster for consecutive stations at a roll-along than for the first one (ABEM, 2008).

Thirty one (31) stainless steel electrodes were driven into the ground with a small hammer at 10 m spacings for the inner (2 and 3) and outer (4) cables respectively (Figures 5a, 5b and 6). The separation was done using a measuring tape. The cables were laid and the end of the fabricated bunch of wires with take-outs separation of 4 m were connected to their respective cable take-outs (Figure 7a). The other ends of the wires with take-outs separation of 10 m were also connected to the corresponding electrodes. The ends of the wires that are to be connected to the cables were painted red to distinguish them from the ends to be connected to the electrodes (Figure 7b). The paintings also speed up the work because the wires were rolled in the desired directions.

The thirty one electrodes were connected to the odd-numbered take-outs at electrode separation of 10 m making a total length of 300 m for the first set of measurements using the GRAD4LX8. Cables 3 and 4 were connected using a cable joint with the groove facing the equipment. Cable 1 was not connected during the first set of measurements. The ABEM terrameter, the electrode selector ES 10-64C and the 12 V car battery were then connected between cables 2 and 3 of the set-up. The electrode resistance test was run first before the measurements to ensure that all the 31 electrodes were connected and conducting. In some cases the electrode test failed and water had to be poured under those electrodes and they were also hammered deeper to ensure they pass the electrode test. At the same time as the measurements of the GRAD4LX8 was going on, twenty electrodes were fixed midway in-between the electrodes of cables 2 and 3; this is for the GRAD4S8 measurements.

The GRAD4S8 measurements were carried out after the GRAD4LX8 one. Electrode test was also carried out for this short layout of forty one electrodes spaced 5 m apart (total length 200 m) before the measurements. The profiles had a minimum electrode spacing of 5 m, and a minimum profile length of 400 m and a maximum of 1,200 m (using the roll along technique). The roll-along technique (Dahl and Schultz, 2001) was used to cover the entire length of the profiles where necessary.

The roll-along technique (Figure 6) was employed on all the profiles in order to extend horizontally the area to be covered by the survey. Whilst the measurements were going on for the long lay out, twenty electrodes were fixed, ten of them midway between the electrodes in cable 4 and the rest at 10 m interval beyond the 4. It was not possible to just move one cable past the end of the cable towards the crater rim after the first set of measurements, because of the modification of the cable. The inner cables have 20 short extended wires (length between 4 and 61 m) (Table 1) whereas the outer cables have 11 long extended wires (length between 61 and 121 m) (Table 2). The

whole set up has to be dismantled and moved 100 m towards the crater rim to be reconnected.

At the second, third and all the subsequent measurement stations, so long as the profile was being extended, all the four cables were used for the GRAD4LX8 giving a total length of 400 m. Cable joints were used to connect first and second cables and the third and fourth cables and the groove on the cable joint used to connect them were facing the station. The terrameter, the electrode selector ES 10-64C and the 12 V car battery were connected between the second and third cables. The procedure described for the first set of measurements were repeated to acquire the data. The wires and in some cases the cables were tied to trees (mainly cocoa trees) with ropes so that they do not drift down the steep slope especially near the rim of the crater. At some points jumpers were joined so that wires could be connected to the electrode. GPS readings were taken at 10 m intervals.

Bad data points were easily viewed as they appeared as stand out points because the values were displayed in the form of profiles for each data level. These bad data points could be due to the failure of the relays at one of the electrodes, poor electrode ground contact due to dry, sandy or stony ground, attaching electrodes to wrong connectors, or shorting across the cables due to very wet ground conditions especially close to the lake shore. Change settings/Use finite element method was used to calculate the apparent resistivities because all the data contained topography. The L_1 norm (robust inversion) was employed. The L_1 norm also gives more stable results (Zhou and Dahlin, 2003; Dahlin and Zhou, 2004). The Gauss-Newton method was used in calculating the sensitivity matrix for all the iterations. Talus is common around Lake Bosumtwi when one moves closer to the shore of the lake especially at the western part and this gave large surface variations of resistivity near the ground surface. To get optimum results, the Inversion/Model refinement was used which allows the user to choose models with widths of half electrode spacing. This was necessary because failure to resolve the near surface variations could lead to distortions in the lower portion of the model as the program attempts to reduce the misfit. The downside of this Inversion/Model refinement is the increase in the inversion time. When the root mean square (RMS) error between the present and the previous iterations is $< 0.1\%$ the inversion stops.

5. Results and Discussions

On electrical resistivity tomography, fault zones can be easily delineated because they have lower resistivities than their surroundings as a result of their high permeability and high density of discontinuities. Faults are sometimes characterized by their sharp resistivities contrast with their hosts. When the faults are filled with calcite or quartz they can have higher resistivity than their surroundings. Generally, faults occurring in crystalline environment are less resistive than the surrounding rock (Giocoli et al., 2008; Colella et al., 2004; Diaferia et al., 2006; Scheibz et al., 2009; Suzuki et al., 2000; Barsukov, 1970). The analysis of the resistivity images is based on the knowledge of the geology of the crater area and the topography on the profile. The results in the various communities (figure 8) are discussed in the next section.

5.1. Brodekwano

In this community, the sediments stretch from the shore to the end of the profile. The moderately high resistivity region ($> 90 \Omega.m$) at the base of Figure 9a and the zone marked **P** are likely to represent parautochthonous breccia (brecciated monomict) because of their geometry. It is likely they were part of the target surface marked with the dotted line and faulted at 200 and 350 m. The portion labeled **F** is probably an open fracture filled with clasts. The faults identified at 200 and 450 m have different dip orientations.

5.2 Dwamam

The Dwamam profile (Figure 9b) exhibits peculiar characteristics; the topography rises sharply from the shore of the lake to about 180 m and descends to about 20 m and almost flattens. From the field observation there were no lake sediments from 5 m mark to about 200 m from the shore. The ERT very clearly shows the location of the lake sediments from 200 m to about 500 m mark being in very good agreement with the field observations. The region between 200 – 500 m (rectangle with solid black line) which lies between two moderately high resistivity regions ($> 64 - 200 \Omega.m$) could represent a down-thrown region which was later filled by sediments. The zones marked **P** at the shore were interpreted as in-situ blocks (parautochthonous) that have been faulted and those at 600 and 900 m as brecciated monomict because of their geometry. The open fractures **F** are possibly filled with clasts.

5.3. Duase

The moderately high resistivity regions marked **D** on figure 9c could be dikes due to their structure and their resistivity. They could also have resulted from an in-situ fractured mega-block and as such, parautochthonous breccia. If they are dikes, then they contravene the findings of Hunze and Wonik (2007) that dike breccias have dimensions between one decimeter and one meter. The fractured zone **F** is probably filled with heterogeneous polymict matrix and **A** is a brecciated monomict considering its geometry and dimension. The sediments stretch about to about 900 m on this profile.

5.4. Obo

The high resistivity region ($> 128 \Omega.m$) at the base of the image (Figure 10a) is likely to represent the meta-sedimentary target rock, because of its geometry and lateral extent (hundreds of meters) and high resistivity. The zone marked **P** is likely to represent a brecciated monomict. This profile shows high resistivities on the surface which could be talus eroded from the upper crater walls and brought there by mass wasting.

5.5. Adwafo

The moderately low resistivity region ($< 64 - 100 \Omega.m$) observed on the surface of the profile (Figure 10b) could come from the considerable amount of talus found in the area. The region **P** is possibly a brecciated monomict and part of the target rock. The high resistivity region ($> 128 \Omega.m$) observed at the base from 380 to 620 m is likely to represent the meta-sedimentary target rock, because of its high resistivity and geometry, and it is possible that this target rock has been faulted at point 500 m resulting in a down-throw. The patches of high resistivity regions near the surface indicated as **A** could either be talus eroded from the upper crater walls and brought there by mass wasting as a result of the steepness of the slope or allochthonous breccia.

5.6. Esaase

The moderately low resistivity region ($< 64 - 100 \Omega.m$) observed on the surface of the profile (Figure 10c) could come from the considerable amount of talus found in the area. The zones marked **A** could be interpreted as allochthonous breccia or talus eroded from the upper crater walls and brought there by mass wasting. The feature at the base of the profile with resistivity $> 128 \Omega.m$ is likely to represent the meta-sedimentary target rock, because of its lateral extent (hundreds of meters), high resistivity and geometry. The faults on this traverse dip very sharply. The extent of the sediments is about 200 m.

6. Conclusion

The 2 m take-out cable of the ABEM LUND Resistivity Imaging System which can probe to a depth of about 30 m when the four cables are connected has been modified to function as 5 m take-out which gives a total length of 400 m and can probe to about 75 m depth. The modification was made possible by joining wires from the take-out points to their respective electrodes. The modified cables have been used successfully at six sites around the 1.07 Ma old Bosumtwi impact crater to obtain information about the subsurface using the multi-electrode gradient array. The results correlate well with geological information.

The electrical resistivity tomography (ERT) clearly shows three formations:

- i. basement metamorphic rocks which are made up of meta-volcanic and meta-sedimentary rocks
- ii. impact related breccias (dikes, parautochthonous and allochthonous) and
- iii. post impact lake sediments deposited during high level stages of the lake history.

The ERTs also highlighted areas characterized by faults, fractures and the impact related breccias such as dikes, parautochthonous and allochthonous. They also provided information on the geometry of the faults (dips and displacement) and the fracture pattern on the target meta-sedimentary and meta-volcanic rocks.

The results on the profiles at Brodekwano and Dwaman in the East and Duase in the Southeast sections of the crater could not delineate the sediment/target rock contact as compared to those of Obo on the North, Adwafo on the Northwest and Esaase on the West. There are two possibilities why the sediment and target rock contact was not intercepted in these areas; first, it is possible that the target rock is far below the depth of resolution of the set up and/or second, the target has been greatly fractured and so was not well resolved. The faults in the western and north-western section of the crater are steeper than those on the east and south-east. The results show that with the multi-electrode system, the cables can be modified to suit the geological conditions and requirements. The ERT technique has also proved useful in mapping the subsurface structure of the crater thus highlighting the utility of this technique in impact cratering studies. The methodology presented in this paper offers a new technique to modify existing multi-electrode cables for geo-electrical studies.

Acknowledgements

The research was funded by Kwame Nkrumah University of Science and Technology (KNUST), Kumasi, and Laboratoire IDES- UMR 8148, Université Paris Sud and the French Embassy, Ghana. We wish to thank the Bosumtwi District Assembly, Ghana for granting our research. We also thank the students and service personnels at KNUST, and all the people in the communities around Lake Bosumtwi who helped us to acquire the data.

References

- ABEM, A. I. (2008). *Instruction manual, Terrameter SAS4000/SAS1000*.
- Barsukov, O. M. (1970). Relationship between the electrical resistivity of rocks and tectonic processes, *Izv. Acad. Sci., USSR Phys. Solid Earth, Engl. Transl.* (1), 55–59.

- Boamah, D. and C. Koeberl (2003). Geology and geochemistry of shallow drill cores from the Bosumtwi Impact Structure, Ghana. *Meteoritics and Planetary Science* 38, 1137–1159.
- Colangelo, G., V. Lapenna, A. Loperte, A. Perrone, and L. Telesca (2008). 2D electrical resistivity tomographies for investigating recent activation landslides in Basilicata Region (Southern Italy). *Annals of Geophysics* 51(1), 275–285.
- Colella, A., V. Lapenna, and E. Rizzo (2004). High-resolution imaging of the high Agri valley basin (Southern Italy) with the electrical resistivity tomography. *Tectonophysics* 386(1-2), 29–40.
- Coney, L., R. L. Gibson, W. U. Reimold, and C. Koeberl (2007). Lithostratigraphic and petrographic analysis of ICDP drill core LB-07A, Bosumtwi Impact Structure, Ghana. *Meteoritic and Planetary Science* 42(4/5), 569–589.
- Dahl, J. M. and P. H. Schultz (2001). Measurement of stress wave asymmetries in hypervelocity projectile impact experiments. *International Journal of Impact Engineering* 26, 145–155.
- Dahlin, T. and B. Zhou (2004). A numerical comparison of 2D resistivity imaging with ten electrode arrays. *Geophysical Prospecting* 52, 379–398.
- Dahlin, T. and B. Zhou (2006). Multiple-gradient array measurements for multichannel 2D resistivity imaging. *Near Surface Geophysics*, 113–123.
- Deutsch, A., S. Luetke, and V. Heinrich (2007). The ICDP Lake Bosumtwi impact crater scientific drilling project (Ghana): Core LB-08A litho-log, related ejecta, and shock recovery experiments. *Meteoritics and Planetary Science* 42(4/5), 635–654.
- Diaferia, I., M. Barchi, M. Loddo, D. Schiavone, and A. Siniscalchi (2006). Detailed imaging of tectonic structures by multiscale earth resistivity tomographies: The Colfiorito normal faults (Central Italy):. *Geophysical Research Letters* 33(9), L09305.1–L09305.4.
- Giocoli, A., C. Magri, P. Vannoli, S. Piscitelli, E. Rizzo, A. Siniscalchi, P. Burrato, C. Basso, and C. D. Nocera (2008). Electrical resistivity tomography investigations in the Ufita Valley (Southern Italy). *Annals of Geophysics* 51(1), 213–223.
- Griffiths, D. H. and R. D. Barker (1993). Two-dimensional resistivity imaging and modelling in areas of complex geology. *Journal of Applied Geophysics* 29, 211–226.
- Gunther, T., C. Rucker, and K. Spitzer (2006). Three dimensional modeling and inversion of dc resistivity data incorporating topography—II Inversion. *Geophysical Journal International* 166, 506–517.
- Hunze, S. and T. Wonik (2007). Lithological and structural characteristics of the Lake Bosumtwi Impact Crater, Ghana: Interpretation of acoustic televiewer images. *Meteoritics and Planetary Science* 42(4/5), 779–792.
- Karp, T., B. Milkereit, P. Janle, S. K. Danuor, J. Pohl, H. Berckhemer, and C. A. Scholz (2002). Seismic investigation of the Lake Bosumtwi impact crater: Preliminary results. *Planetary and Space Science* 50, 735–743.
- Koeberl, C. and W. U. Reimold (2005, June). Bosumtwi Impact Crater, Ghana (West Africa): An Updated and Revised Geological Map, with Explanations. *Jahrbuch der Geologischen Bundesanstalt* 145(1), 31–70.
- Lapenna, V., P. Lorenzo, A. Perrone, S. Piscitelli, E. Rizzo, and F. Sdao (2005). Case history: 2D electrical resistivity imaging of some complex landslides in Lucanian Apennine (Southern Italy). *Geophysics* 70(3), B11–B18.
- Loke, M. H. and R. D. Barker (1996). Rapid least-squares inversion of apparent resistivity pseudosections by a quasi-Newton method. *Geophysical Prospecting* 44, 131–152.
- Moon, P. A. and D. Mason (1967). The geology of 1/4⁰ field sheets 129 and 131, Bompata S.W. and N.W. *Ghana Geological Survey Bulletin* 31, 1–51.
- Scheibz, J., H. Haeusler, G. Kardeis, F. Kohlbeck, W. Chwatal, H. Figdor, and C. Koenig (2009). Geologic interpretation of geophysical investigations in the Oslip section, Rust Range, Northern Burgenland, Austria, in European Geosciences Union: Vienna, Austria. *Geophysical Research Abstracts* 11, 10559.
- Scholz, C. A., T. Karp, and R. P. Lyons (2007). Structure and morphology of the Bosumtwi impact structure from seismic reflection data. *Meteoritic and Planetary Science* 42(4/5), 549–560.
- Steeple, D. W. (2001). Engineering and environmental geophysics at the millennium. *Geophysics* 66, 31–35.
- Suzuki, K., S. Toda, K. Kusunoki, Y. Fujimitsu, T. Mogi, and A. Jomori (2000). Case studies of electrical and electromagnetic methods applied to mapping active faults beneath the thick Quaternary. *Engineering Geology* 56(1-2), 29–45.
- Tong, C. H., C. Lana, Y. R. Marangoni, and V. R. Elis (2010). Geoelectric evidence for centripetal resurgence of impact melt and breccias over central uplift of Araguainha impact structure. *Geology* 38, 91–94.
- Zhou, B. and T. Dahlin (2003). Properties and effects of measurement errors on 2D resistivity imaging surveying. *Near Surface Geophysics* 1, 105–117.

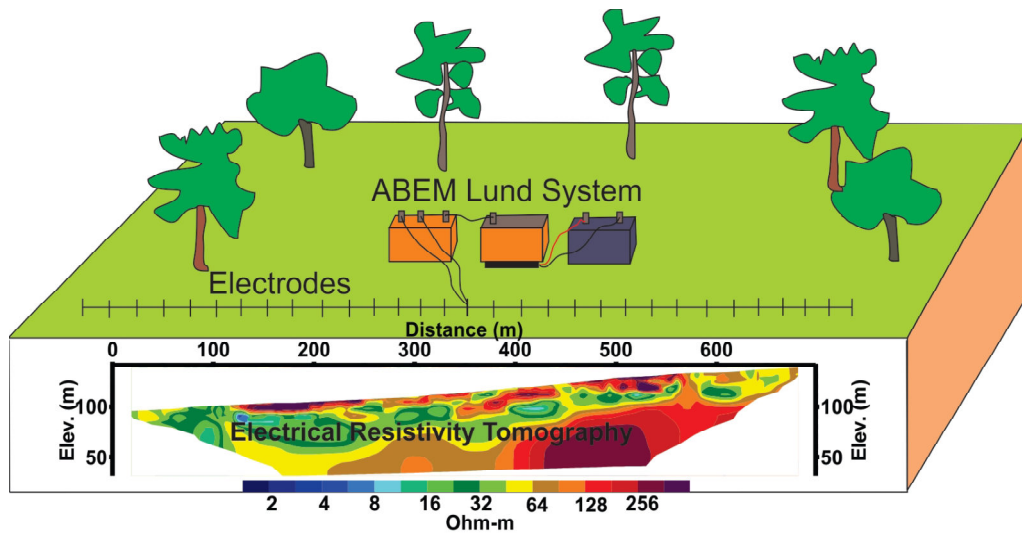


Figure 1. Sketch of multi electrode array showing the set-up and a possible electrical resistivity tomography (ERT) model obtained after inversion.

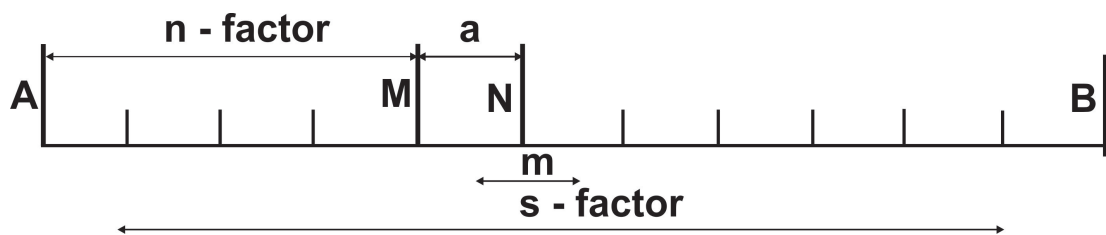


Figure 2. Sketch of gradient array showing the position of the electrodes for a measurement with a current-electrode separation of $(s + 2)a$, where separation factor $s = 9$, the $n = 4$, n is the smallest relative spacing between a current electrode and a potential electrode and the midpoint factor $m = -1$ (Dahlin and Zhou, 2006).

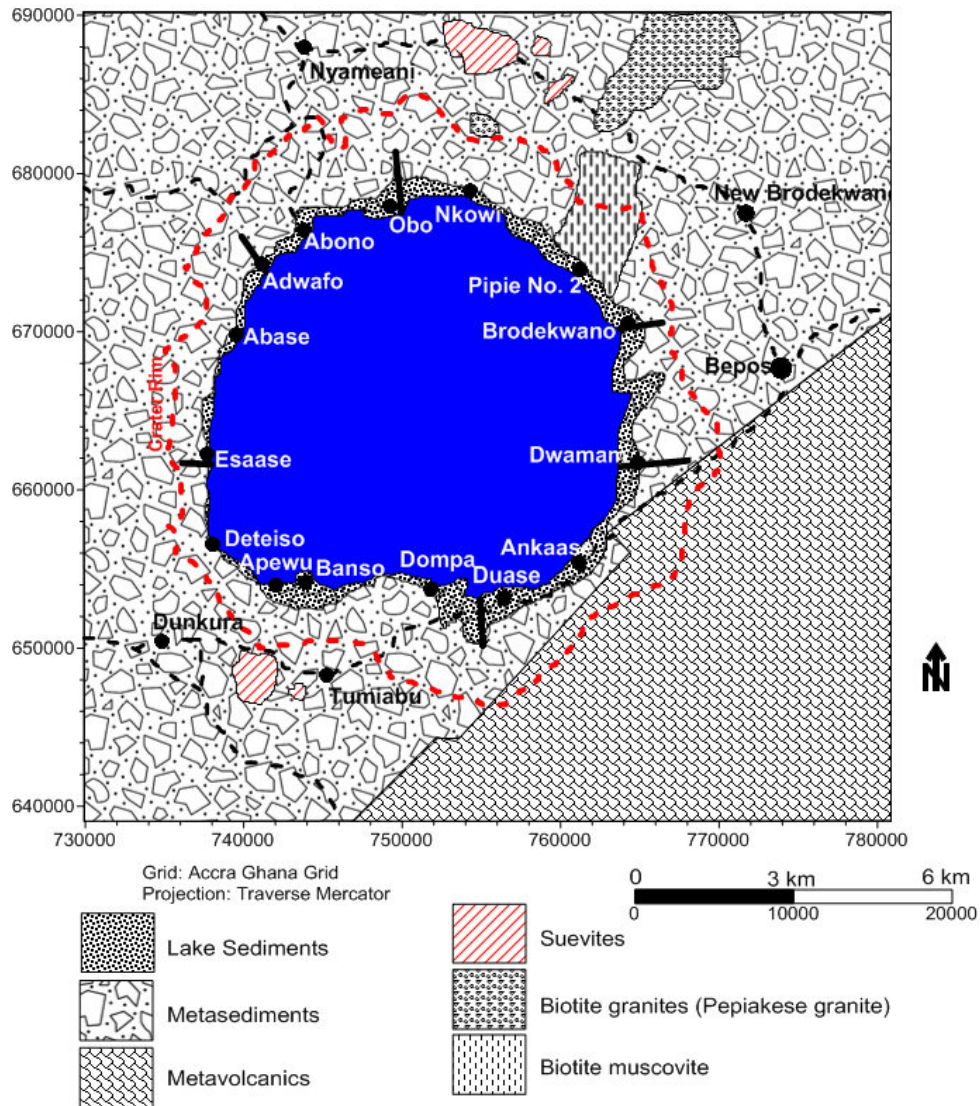


Figure 3. Geological map of Bosumtwi crater area with the profiles in black (Modified from Koerberl and Reimold, 2005).

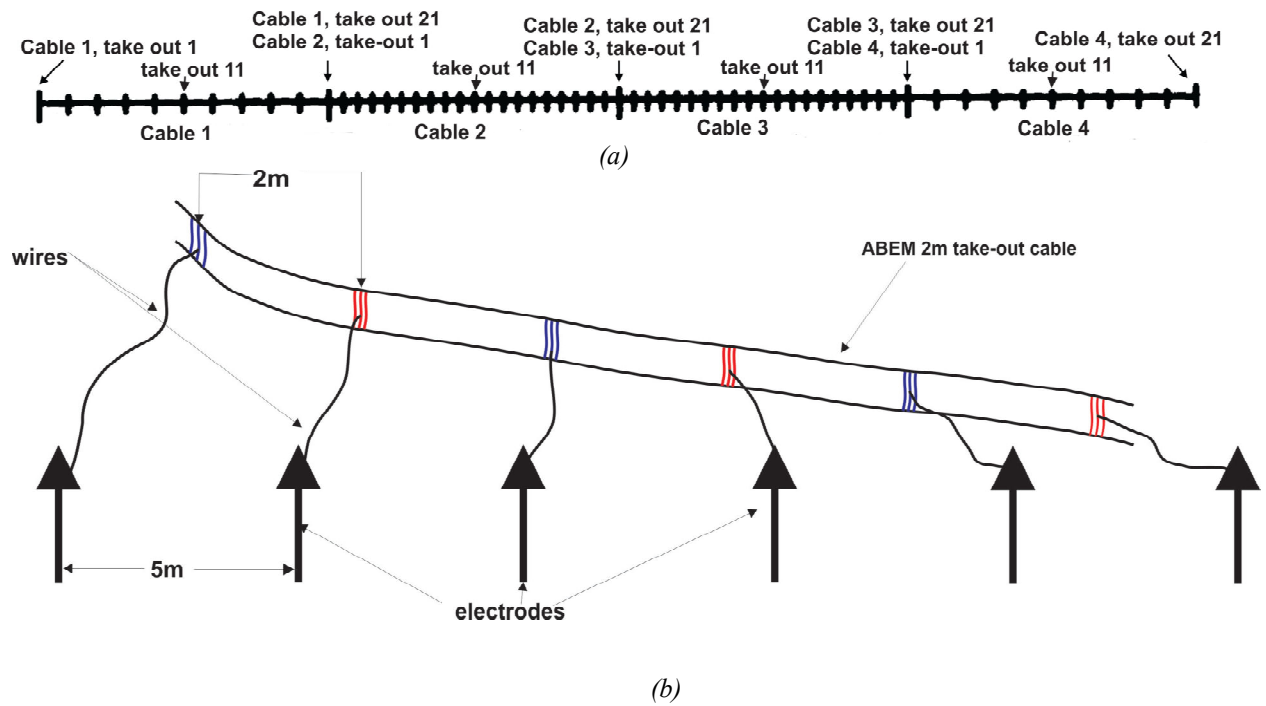


Figure 4. Sketch of the (a) layout of the four cables (b) modified 2 m take-out ABEM cable and its connection

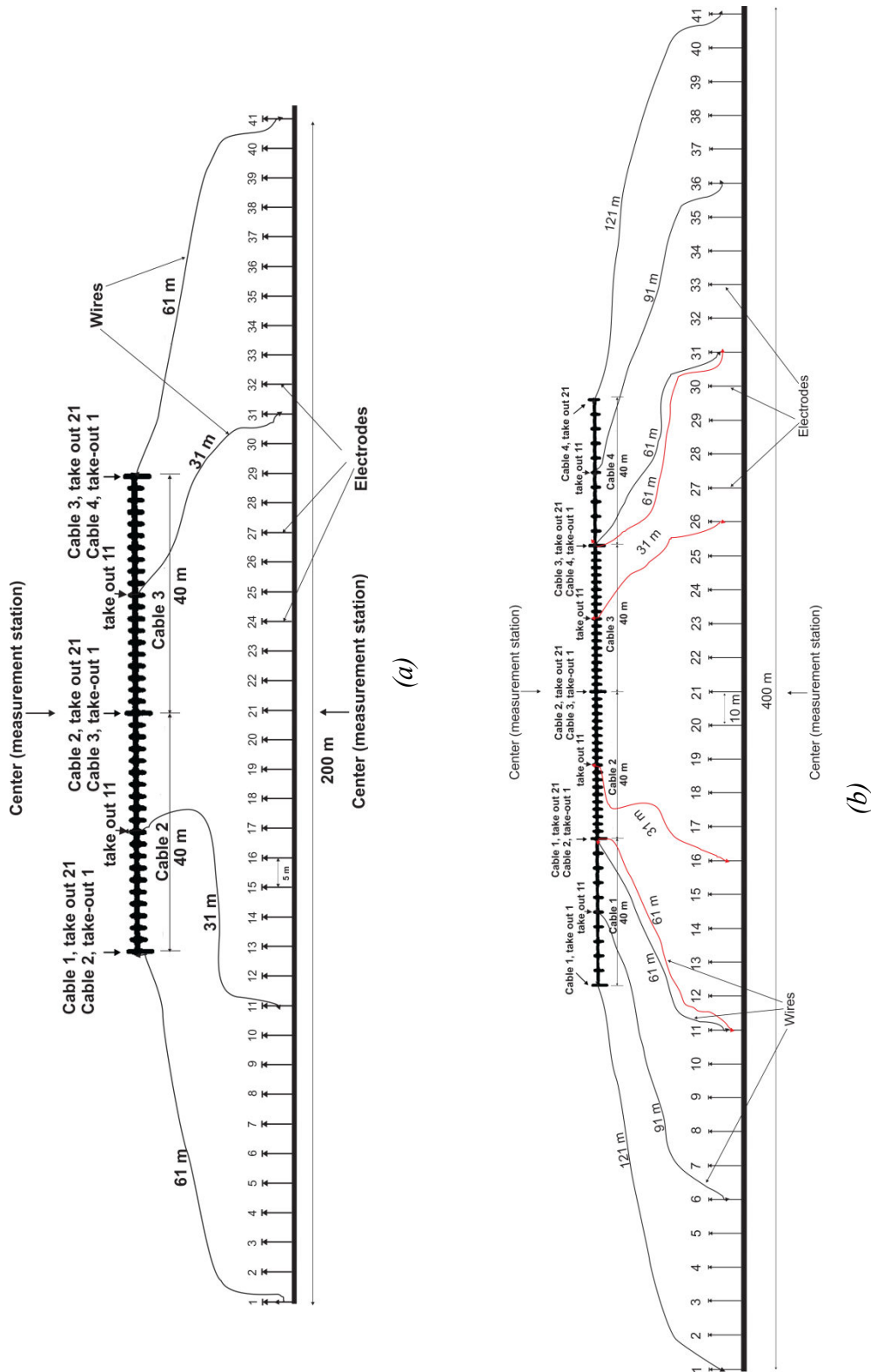


Figure 5 – Sketch of the connection for (a) short layout (GRAD4S8) and (b) long layout (GRAD4LX8). The red wires are used for both the long and short layout measurements

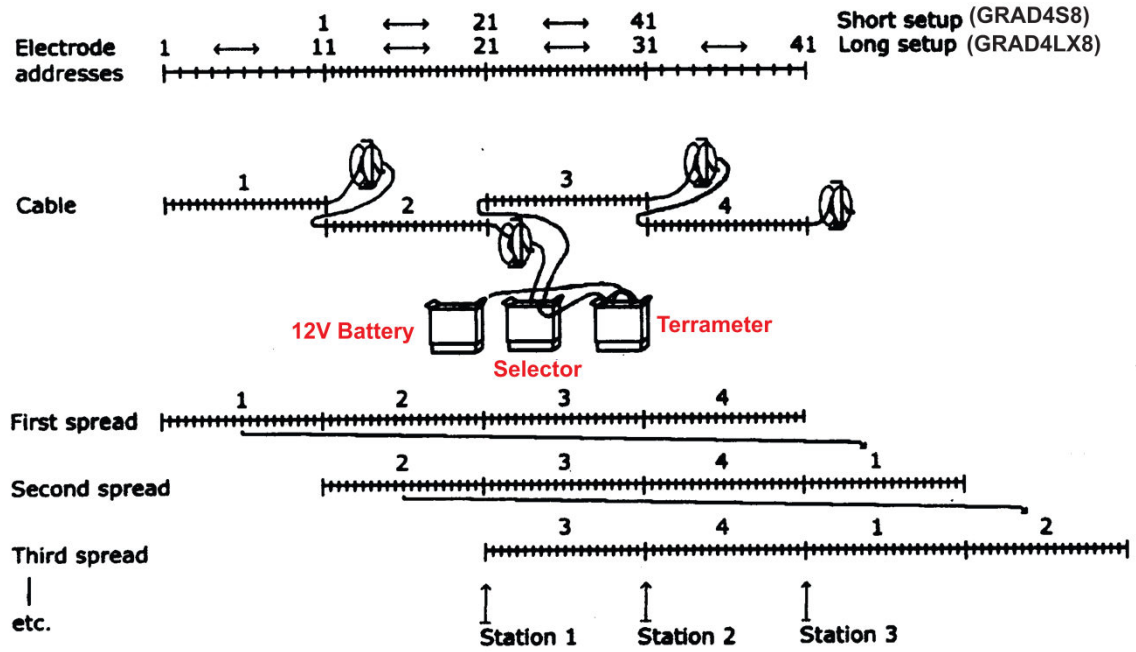


Figure 6 – Roll-along technique using four electrode cables (modified from ABEM, 2008)



Figure 7 – (a) A jumper connecting a wire and the ABEM 2 m take-out cable and (b) a jumper connecting a wire to an electrode.

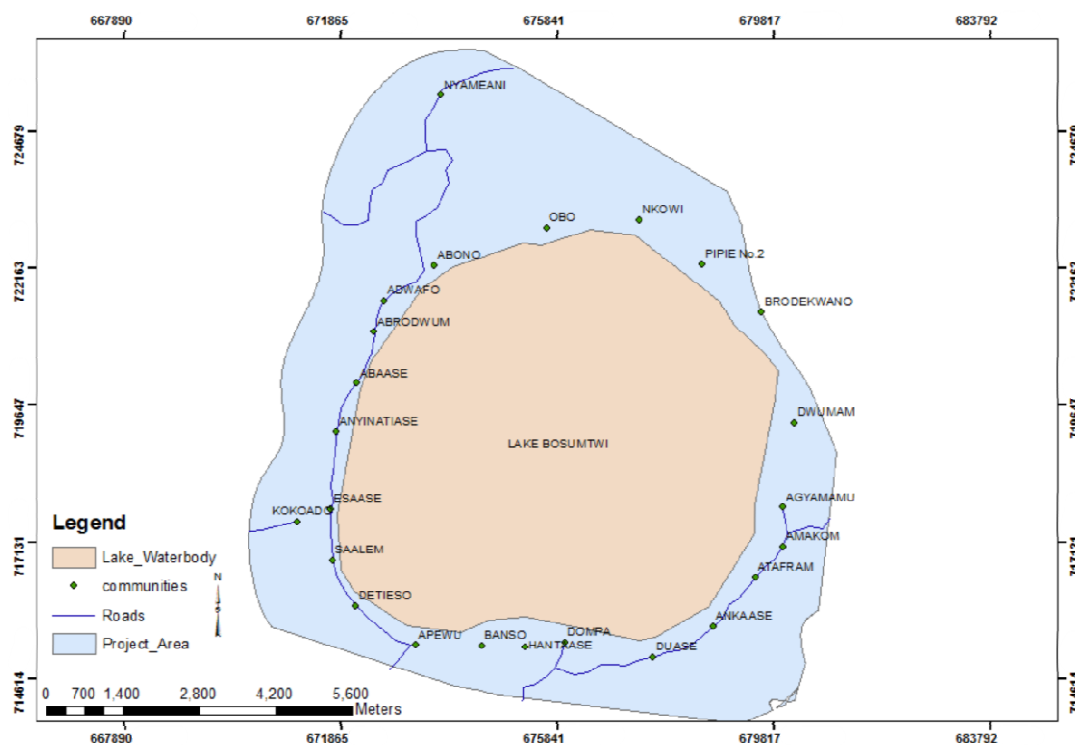


Figure 8. Map showing the communities around the lake.

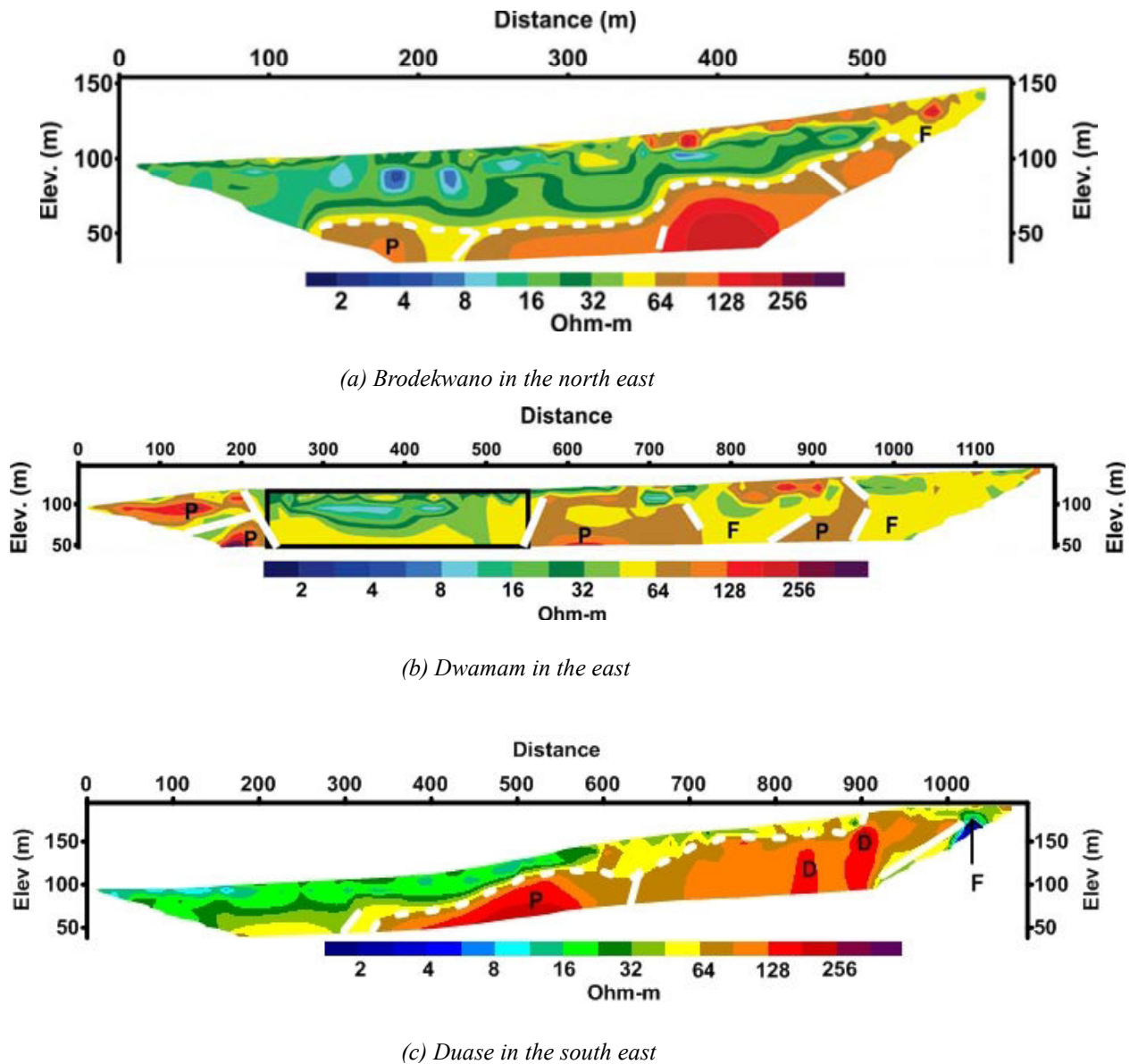
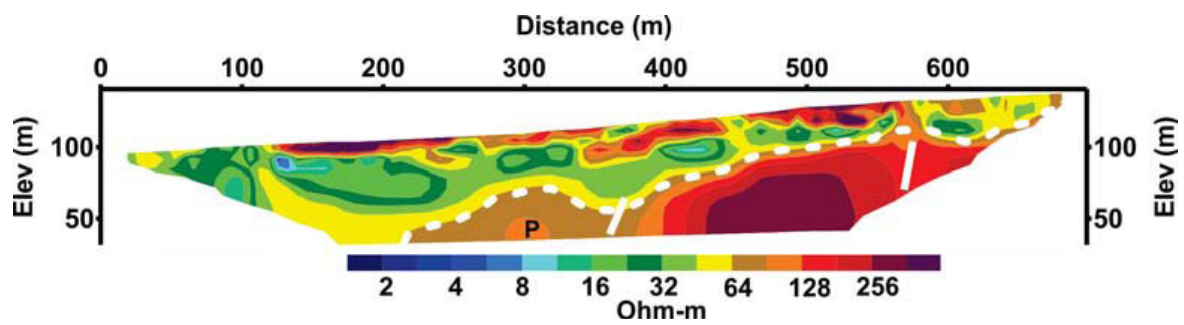
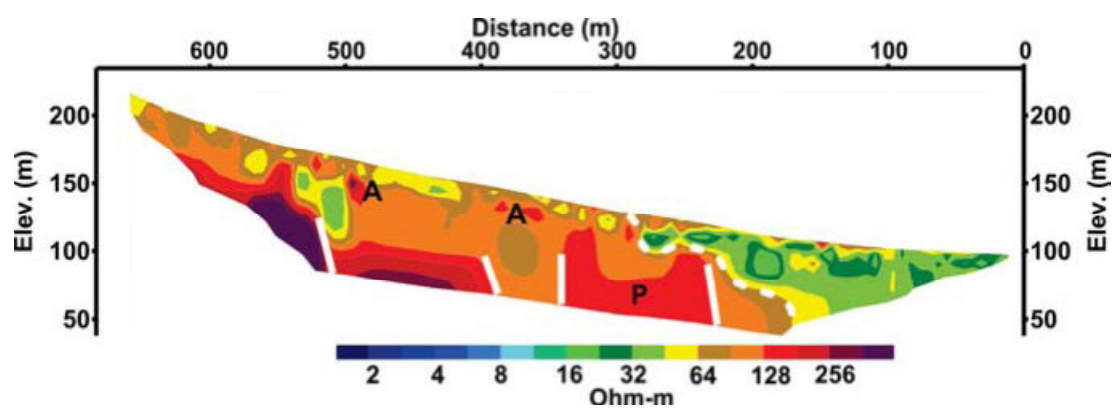


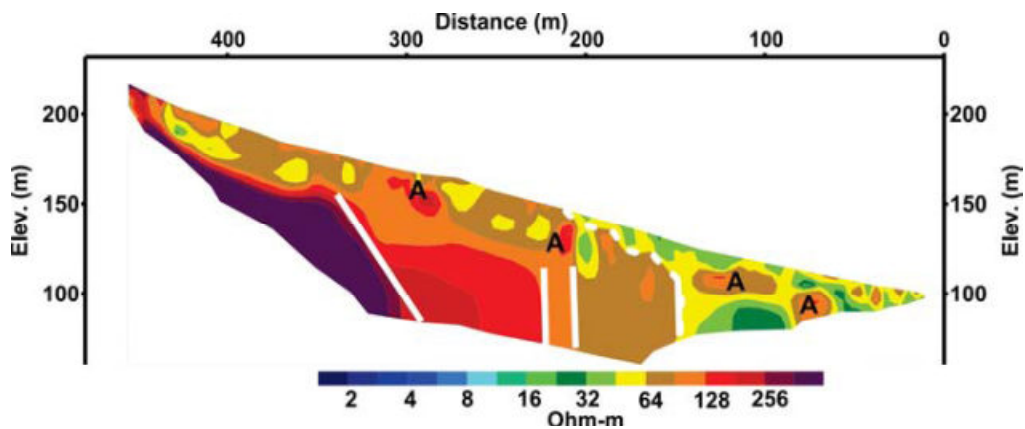
Figure 9. 2D resistivity images on the eastern and southern sections of the lake: (a) Brodekwano in the north east; (b) Dwamam in the east; and (c) Duase in the south east



(a) Obo in the north



(b) Adwafo in the north west



(c) Esaase in the south west

Figure 10. 2D resistivity images on the northern and western sections of the lake: (a) Obo in the north; (b) Adwafo in the north west; (c) Esaase in the south west

Table 1 – Length of the wires for the 2 inner cables

Cable 4 take-out	Cable 1 take-out	Take-out separation (m)	Electrode position (m)	Difference in length (m)	Actual length of wire (m)
1	21	0	0	0	0
2	20	2	5	3	4
3	19	4	10	6	7
4	18	6	15	9	10
5	17	8	20	12	13
6	16	10	25	15	16
7	15	12	30	18	19
8	14	14	35	21	22
9	13	16	40	24	25
10	12	18	45	27	28
11	11	20	50	30	31
12	10	22	55	33	34
13	9	24	60	36	37
14	8	26	65	39	40
15	7	28	70	42	43
16	6	30	75	45	46
17	5	32	80	48	49
18	4	34	85	51	52
19	3	36	90	54	55
20	2	38	95	57	58
21	1	40	100	60	61

Table 2 – Length of the wires for the 2 outer cables

Cable 4 take-out	Cable 1 take-out	Take-out separation (m)	Electrode position (m)	Difference in length (m)	Actual length of wire (m)
1	21	40	100	60	61
3	19	44	110	66	67
5	17	48	120	72	73
7	15	52	130	78	79
9	13	56	140	84	85
11	11	60	150	90	91
13	9	64	160	96	97
15	7	68	170	102	103
17	5	72	180	108	109
19	3	76	190	114	115
21	1	80	200	120	120

Table 3 – Number of data points for 4 cable layout (ABEM, 2008)

Array type	Protocol name	Address	No. of file	No. of data ORG data UP	Total data for one layout
Gradient	GRAD4LX8	LONG	608	340	1080
	GRAD4S8SHORT		248	160	